

Which parameters are optimal? - A comprehensive numerical analysis of background phase correction with SHARP

Ferdinand Schweser¹, Pınar Senay Özbay^{2,3}, Andreas Deistung¹, Edsel Daniel Peres Gomez¹, Xiang Feng¹, Daniel Nanz², and Jürgen R Reichenbach¹

¹Medical Physics Group, Institute of Diagnostic and Interventional Radiology I, Jena University Hospital - Friedrich Schiller University Jena, Jena, Germany,

²Department of Radiology, University Hospital Zurich, Zurich, Switzerland, ³Institute for Biomedical Engineering, University and ETH Zurich, Zurich, Switzerland

TARGET AUDIENCE – Researchers interested in background field correction of MR phase images using SHARP.

PURPOSE – Quantitative susceptibility mapping (QSM) is a recent MR post-processing technique with promising research and clinical applications in various fields^{1,2}. One of the most important processing steps of QSM is the elimination of background field contributions that result from susceptibility interfaces outside of the region of interest, such as tissue-air interfaces³. Sophisticated harmonic artifact reduction for phase data³ (SHARP) is regarded as one of the most important techniques in this area. While SHARP exploits mathematical properties of the field and is, thus, in principle parameter-free, two numerical parameters nevertheless need to be defined: The radius of the spherical convolution kernel and a regularization parameter (which depends on the radius⁴). The influence of these parameters has not been investigated in detail so far and they are usually chosen empirically, which may have serious consequences for the comparability of studies relying on SHARP processed phase images. We performed a **comprehensive analysis of the impact of different parameter choices** on the resulting images and propose a **universal definition of the regularization parameter** that does not depend on the spherical radius or on the image resolution. In addition, we show that in some situations the **effective threshold** (i.e. the numerically applied threshold) may deviate from the nominally defined one, and that this discrepancy can be minimized to arbitrary degree by zero-padding in the spatial domain.

THEORY – *Universal regularization*: We propose to replace the truncated singular value decomposition (TSVD) regularization of the deconvolution step of SHARP by simple high-pass filtering. This is justified because the SHARP deconvolution kernel (the basis of TSVD) is smooth and radial symmetric in the center of the Fourier space. TSVD is, consequently, equivalent to high-pass filtering if the SVD truncation value is sufficiently low (which is true for SHARP). The thresholding parameter used in the present work defines the cut-off frequency of the high-pass filter in mm^{-1} . Compared to the TSVD threshold this new definition of the regularization parameter is invariant to the radius of the spherical shell, image resolution and FOV, and may, thus, be used universally. *Effective regularization threshold*: Due to the direct relation between the size of the FOV and the discretization of the Fourier domain, a small FOV results in a coarse Fourier domain and, thus, also discretizes the effective regularization parameter. In a small-FOV scenario the effective threshold may substantially deviate from the desired threshold as illustrated in **Figure 4**. Therefore, we recommend to zero-pad small FOV data in one or more dimensions (e.g. small number of slices) prior to applying SHARP.

METHODS – *Numerical model*: We used a detailed numerical anatomical brain model for the analysis to be able to compare against a gold standard reference. The model was created from T_1 -weighted volunteer data ($1 \times 1 \times 1 \text{ mm}^3$) via automatic segmentation (FreeSurfer¹⁰) with manual segmentation of venous vessels. To include field contributions from the torso the brain model was embedded into the skull of a human whole-body model of The Virtual Family (Duke, 1 mm^3) and typical magnetic susceptibilities were assigned. A reference model with no background distortions was generated from the brain tissue model (without skull and bone) embedded in susceptibility equal to the mean value of the brain's susceptibility (**Fig. 1** right). To avoid unrealistic sharp interfaces between different tissue types the susceptibility models were smoothed with a 3D Gaussian kernel (std-width 0.42 mm). The field perturbations of the models were computed by fast-forward field computation⁵ and phase accumulation was calculated for $B_0 \cdot TE = 60 \text{ T} \cdot \text{ms}$. Brain tissue defined the region of measurable MR phase. In addition, voxels with an estimated phase variation throughout the voxel of more than 6 rad were also regarded as not measurable due to rapid intravoxel spin dephasing⁶ ($TE > 3 \cdot T_2'$). Noise was not added to the model because noise was regarded to be irrelevant for the analysis. *Application of SHARP*: We applied SHARP with successively decreasing radii towards the surface of the brain⁹. Prior to SHARP processing the models were zero-padded to a FOV of $451 \times 451 \times 451 \text{ mm}^3$ to avoid discretization artifacts (see above). SHARP was applied with different maximum radii between 1 and 15 voxels (in steps of 1 voxel) and regularization thresholds between 0 and 0.05 (all possible discretized values). *Calculation of susceptibility maps*: To analyze the impact of incomplete background removal on the field-to-susceptibility inversion a spatial domain QSM algorithm⁷ was applied based on LSQR (maximum 150 iterations; no explicit regularization; tolerance 10^{-5}). *Analysis*: The root mean squared error (RMSE) was calculated with respect to the gold standard phase (**Fig. 1**, middle) and gold standard susceptibility map (**Fig. 1**, right), respectively, for all resulting images over the whole brain and, additionally, only within a certain distance from the brain's surface ($\pm 1 \text{ mm}$; distances: 1 to 30 mm).

RESULTS – The color-coding in **Figure 2** shows the minimal (best) RMSE obtained at different distances from the brain's surface with different spherical radii. The minimum RMSE generally decreased toward the center of the brain. Maximum radii around 9 voxels provided the smallest RMSEs (Fig. 2). Closer than 9 mm to the brain's surface the minimum error increased rapidly for all parameter settings. **Figure 3** shows the total RMSE (over the whole brain) as a function of threshold and maximum radius. The region of minimum RMSE in the phase (left image) is centered at a radius of 10 voxels (vx) and a threshold of 0.009 mm^{-1} . The RMSE of the susceptibility maps shows a similar pattern. However, the RMSE of the susceptibility maps (right image) was slightly less sensitive towards lower thresholds compared to the phase.

DISCUSSION – The quality of SHARP phase images is a trade-off between two types of artifacts: If the regularization threshold is chosen too small artifacts are dominated by contributions due to the violation of an implicit mathematical boundary assumption in SHARP⁸. If the regularization parameter is chosen too high, too much of low frequency information is removed from the images. The relative insensitivity of the susceptibility mapping with respect to small regularization parameters (Fig. 4 right) may be explained by the ability of the inversion algorithm to explain residual background fields as magnetic susceptibility outside or at the surface of the brain. The optimal spherical radius of 9-10 voxels is in line with empirical reports in the literature⁵.

CONCLUSION – The proposed novel regularization scheme allows using the same regularization parameter irrespective of other image parameters like image resolution. The optimal parameter choice for QSM with SHARP is a maximum radius of 10 voxels and a regularization parameter below 0.01 mm^{-1} (**Fig. 3**). Zero-padding of the phase prior to SHARP ensures that effective and desired regularization parameters coincide if the number of acquired slices is low (small FOV in slice direction; **Fig. 4**).

REFERENCES – [1] Duyn J, 2013. *J Magn Reson.* 229:198-207. [2] Reichenbach JR, 2012. *NeuroImage*. 62(2):1311-5. [3] Schweser F et al., 2011. *ISMRM p2667*. [5] Marques JP and Bowtell RW, 2005. *Concepts Magn Reson B Magn Reson Eng.* 25B(1):65-78. [6] Johnson G and Hutchison JMS, 1985. *J Magn Reson.* 63:14-30. [7] Schweser F et al., 2010. *Med Phys.* 37(10):5165-78. [8] Sun H and Wilman AH, 2013. *J Magn Reson Med* (epub). [9] Li W et al., 2011. *NeuroImage*, 55(4):1645-56. [10] Fischl D et al., 2002. *Neuron*. 33(3):341-55

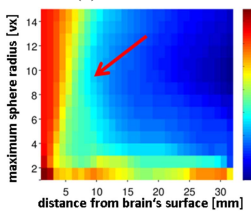


FIGURE 2. Minimum RMSE (color-coding; in rad) of the background-corrected phase over all regularized parameters as a function of the distance from the brain's surface (x-axis; in mm) and the maximum sphere radius (y-axis; in vx).

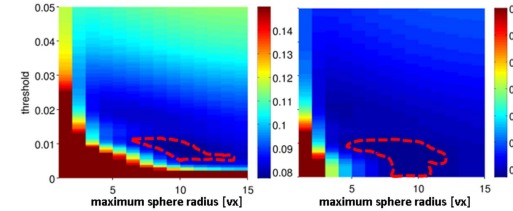


FIGURE 3. Left: Total RMSE (color-coding; in rad) of the background-corrected phase as a function of the maximum sphere radius (x-axis; vx) and the regularization threshold (y-axis; mm⁻¹). Right: Corresponding figure of the RMSE (ppm) of susceptibility maps calculated from the background corrected phase images. The dotted red line marks the optimal parameter set.

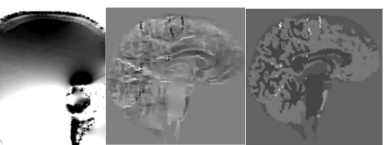


FIGURE 1. Numerical model. **Left:** Simulated phase (input) with background contributions from the whole body model [-10...10 rad]. **Middle:** Reference phase without background fields [-1...1 rad]. **Right:** Reference susceptibility distribution [-0.1...0.2 ppm].

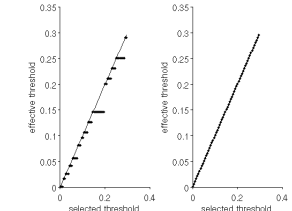


FIGURE 4. Effective threshold vs. selected threshold. Left: Effective threshold as a function of the chosen threshold for a small FOV of $129 \times 129 \times 31 \text{ mm}^3$. Right: Corresponding plot for a larger FOV of $451 \times 451 \times 451 \text{ mm}^3$.